Stem Cell Reports
Article

OPEN ACCESS

Human Neural Stem Cell Transplantation Rescues Functional Deficits in R6/2 and Q140 Huntington's Disease Mice

Jack C. Reidling,[1,11] Aroa Relaño-Ginés,[2,11] Sandra M. Holley,[3,11] Joseph Ochaba,[4] Cindy Moore,[5] Brian Fury,[6] Alice Lau,[7] Andrew H. Tran,[1] Sylvia Yeung,[1] Delaram Salamati,[1] Chunni Zhu,[2] Asa Hatami,[2] Carlos Cepeda,[3] Joshua A. Barry,[3] Talia Kamdjou,[3] Alvin King,[4] Dane Coleal-Bergum,[6] Nicholas R. Franich,[2] Frank M. LaFerla,[1,4] Joan S. Steffan,[1,7] Mathew Blurton-Jones,[1,4,8] Charles K. Meshul,[5,9] Gerhard Bauer,[6] Michael S. Levine,[3,10] Marie-Francoise Chesselet,[2] and Leslie M. Thompson[1,4,7,8,*]

[1]Institute for Memory Impairment and Neurological Disorders, University of California, Irvine, 3400 Biological Sciences III, Irvine, CA 92697-4545, USA
[2]Department of Neurology, David Geffen School of Medicine, University of California, Los Angeles, 710 Westwood Plaza, Los Angeles, CA 90095-1769, USA
[3]Intellectual and Developmental Disabilities Research Center, Semel Institute for Neuroscience and Human Behavior, David Geffen School of Medicine, University of California, Los Angeles, 760 Westwood Plaza, Los Angeles, CA 90095, USA
[4]Department of Neurobiology & Behavior, University of California, Irvine, 3400 Biological Sciences III, Irvine, CA 92697-4545, USA
[5]Portland VA Medical Center, 3710 SW US Veterans Hospital Road, Portland, OR 97239, USA
[6]Institute for Regenerative Cures, University of California, Davis, 2921 Stockton Boulevard, Sacramento, CA 95817, USA
[7]Department of Psychiatry & Human Behavior, University of California, Irvine, 3400 Biological Sciences III, Irvine, CA 92697-4545, USA
[8]Sue and Bill Gross Stem Cell Center, University of California, Irvine, Gross Hall, Room 3219, 845 Health Sciences Road, Irvine, CA 92697, USA
[9]Oregon Health & Science University, Department of Behavioral Neuroscience, 3181 SW Sam Jackson Park Road, L470, Portland, OR 97239, USA
[10]Brain Research Institute, David Geffen School of Medicine, University of California, Los Angeles, 760 Westwood Plaza, Los Angeles, CA 90095, USA
[11]Co-first author
*Correspondence: lmthomps@uci.edu
https://doi.org/10.1016/j.stemcr.2017.11.005

SUMMARY

Huntington's disease (HD) is an inherited neurodegenerative disorder with no disease-modifying treatment. Expansion of the glutamine-encoding repeat in the Huntingtin (*HTT*) gene causes broad effects that are a challenge for single treatment strategies. Strategies based on human stem cells offer a promising option. We evaluated efficacy of transplanting a good manufacturing practice (GMP)-grade human embryonic stem cell-derived neural stem cell (hNSC) line into striatum of HD modeled mice. In HD fragment model R6/2 mice, transplants improve motor deficits, rescue synaptic alterations, and are contacted by nerve terminals from mouse cells. Furthermore, implanted hNSCs are electrophysiologically active. hNSCs also improved motor and late-stage cognitive impairment in a second HD model, Q140 knockin mice. Disease-modifying activity is suggested by the reduction of aberrant accumulation of mutant HTT protein and expression of brain-derived neurotrophic factor (BDNF) in both models. These findings hold promise for future development of stem cell-based therapies.

INTRODUCTION

Huntington's disease (HD) is an autosomal dominant neurodegenerative disease caused by an expanded CAG repeat encoding a polyglutamine repeat within the Huntingtin protein (HTT) (The Huntington's Disease Collaborative Research Group, 1993). Involuntary movements, progressive intellectual decline, and psychiatric disturbances occur (Ross and Tabrizi, 2011), and neuropathology primarily involves degeneration of medium-sized spiny neurons (MSNs) in the striatum and atrophy of the cortex (Vonsattel and DiFiglia, 1998).

Currently no disease-modifying therapies are available, creating a significant unmet medical need. Effective neurorestorative or neuroregenerative strategies based on human stem cells offers a possible therapeutic strategy (for reviews see Drouin-Ouellet, 2014; Golas and Sander, 2016; Kirkeby et al., 2017). Cognitive and motor benefit in a small subset of HD patients (Rosser and Bachoud-Levi, 2012) and sustained benefit in Parkinson's disease patients (Petit et al., 2014) were observed following human fetal cell transplants. Murine (Blurton-Jones et al., 2009) or human (Ager et al., 2015) neural stem cells provided improvements in learning and memory in Alzheimer's disease mice by increasing endogenous synaptic connectivity. Transplantation of stem cell-derived products have also shown benefit in HD mice (Ebert et al., 2010; Mu et al., 2014; Rossignol et al., 2015), including human MSCs overexpressing brain-derived neurotrophic factor (BDNF) (Pollock et al., 2016), and astrocyte progenitors (Benraiss et al., 2016). However, limited research has evaluated human neural stem cells (hNSCs) in genetic models carrying the CAG repeat expansion, and to date no disease-modifying activity has been ascribed to this approach.

To evaluate the potential efficacy of hNSCs, we transplanted a good manufacturing practice (GMP)-grade human embryonic stem cell (hESC)-derived hNSC line into an HD fragment R6/2 mouse model. Implanted cells provided modification of behavioral phenotypes, survived, and showed potential to differentiate into several neural cell types. hNSCs were electrophysiologically active, rescued some electrophysiological alterations, and were

potentially contacted by mouse host nerve termini. Transplantation also improved motor impairment and cognition in a full-length Q140 HD mouse model. Mechanistically, the accumulation of a high molecular weight HTT species (Ochaba et al., 2016) was substantially reduced by the hNSC treatment in R6/2 mice. Visible inclusions were also lowered in both models. Finally, improvement was associated with increased BDNF.

RESULTS

ESI-017 hNSCs Modify Behavior, Survive, and Differentiate when Transplanted into R6/2 Mice

To evaluate efficacy of hNSC transplantation in a transgenic model of HD, we used exon-1 HTT R6/2 mice (~120 CAG repeats) (Cummings et al., 2012), which display rapidly progressing motor and metabolic deficits and early death (~12–14 weeks) (Mangiarini et al., 1996), and can provide an initial assessment of treatment paradigms in preclinical studies (Hickey and Chesselet, 2003; Hockly et al., 2003).

ESI-017 hNSCs Improve Behavior

A diagram of the manufacturing process and quality control for the GMP-grade hNSC line is described in Figures S1A and S1B. Flow cytometry indicated appropriate staining for hNSC proliferation and pluripotency markers (Figure S1A). Immunocytochemistry confirmed staining for the neural ectodermal stem cell marker Nestin (Figure S1C). ESI-017 hNSCs were acquired as frozen aliquots (UC Davis), thawed, and cultured without passaging using the same media reagents as the GMP facility prior to dosing. Five-week-old mice were dosed by intrastriatal stereotactic delivery of 100,000 hNSCs per hemisphere. Male (M) and female (F) R6/2 and non-transgenic (NT) age-matched littermates and vehicle controls (veh) were included (n = 8 R6/2 hNSC M, 6 R6/2 hNSC F, 7 NT hNSC M, 7 NT hNSC F, 7 R6/2 veh M, 6 R6/2 veh F, 8 NT veh M, and 6 NT veh F). Immunosuppression was administered to all mice. Behavioral analysis was performed and mice were euthanized at age 9 weeks, immediately following behavior testing.

Veh-treated mice developed HD-associated behaviors as described previously (Mangiarini et al., 1996). In brief, behavior of R6/2 mice was indistinguishable from that of NT mice at age 5 weeks. By 8 weeks, neurological abnormalities included progressive stereotypical hindlimb-grooming movements, clasping, and an irregular gait. When lifted by the tail normal mice splay both hind and forelimbs, and if mice clench limbs to their abdomen they are considered to "clasp." A delay in onset of R6/2 clasping was observed in all hNSC-treated mice; veh-treated mice clasped by 3 weeks post implant. No hNSC-treated mice clasped at this time point, and at euthanasia (4 weeks post implant) only 50% of hNSC-treated mice clasped (Figure S2). Two locomotor assays were performed. Rotarod tests the ability to walk on an accelerating rotating rod. hNSC-treated R6/2 mice showed a statistically significant improvement in Rotarod performance (30% improvement 1 week post implant, $p < 0.01$; and 19% 3 weeks post implant, $p < 0.05$) over veh-treated R6/2 mice (Figure 1A). The pole test compares times while descending on a vertical beam; R6/2 mice have a longer latency to descend compared with NT mice. A statistically significant ($p = 0.02$) improvement between R6/2 treatment groups was observed at 4 weeks post implant (25% improvement, Figure 1B). A grip strength meter was also used to assess neuromuscular function and motor coordination, and hNSC treatment produced a significant improvement ($p = 0.02$, 16% improvement, Figure 1C) 4 weeks post implant.

ESI-017 hNSC Survival, Migration, and Differentiation

Mice were euthanized 4 weeks post implant and the brain collected, half of which was post-fixed for histology and half flash frozen for biochemistry. hNSCs primarily clustered around the needle track and remained in the striatum (Figure 1D); some were in the cortex and a few migrated to a niche (corpus callosum/white matter tracts) between the cortical and striatal region (Figure S3). Using human markers SC121 (cytosolic) or Ku80 (nuclear), cells mainly stained with the early neuronal marker doublecortin (DCX) (SC121, Figure 2A merge yellow; Ku80, Figures 2B and 2C). Some cells potentially differentiated toward an astrocytic phenotype (glial fibrillary acidic protein [GFAP]) (Figure 2B). There is also non-human GFAP-positive immunostaining around the implantation site (Figures 2A and 2B) that potentially represents a mouse glial cell scar. The differentiation of hNSCs to neuron-restricted progenitors was confirmed with βIII-tubulin (Figures 2D and S3B) and microtubule-associated protein 2 (MAP-2) (Figures 2E and S3C), but a lack of co-localization with NeuN (Figure 2F) suggests no post-mitotic neurons. Using stereological assessment of Ku80-positive cells in one hemisphere, hNSC implant survival numbers showed an average of 41,323 cells (n = 6, 3 males and 3 females), equivalent to ~41% of the initially transplanted 100,000.

Implantation of ESI-017 hNSCs Prevents Corticostriatal Hyperexcitability in R6/2 Mice

We next evaluated electrophysiological activity. Male and female mice were implanted with 100,000 hNSCs (n = 18) or veh (n = 16) in striatum at 5 weeks. We recorded from hNSCs 4–6 weeks post implant (Figures 3A and 3B) in acute brain slices. hNSCs display basic neuronal properties characteristic of immature cells, a significantly smaller

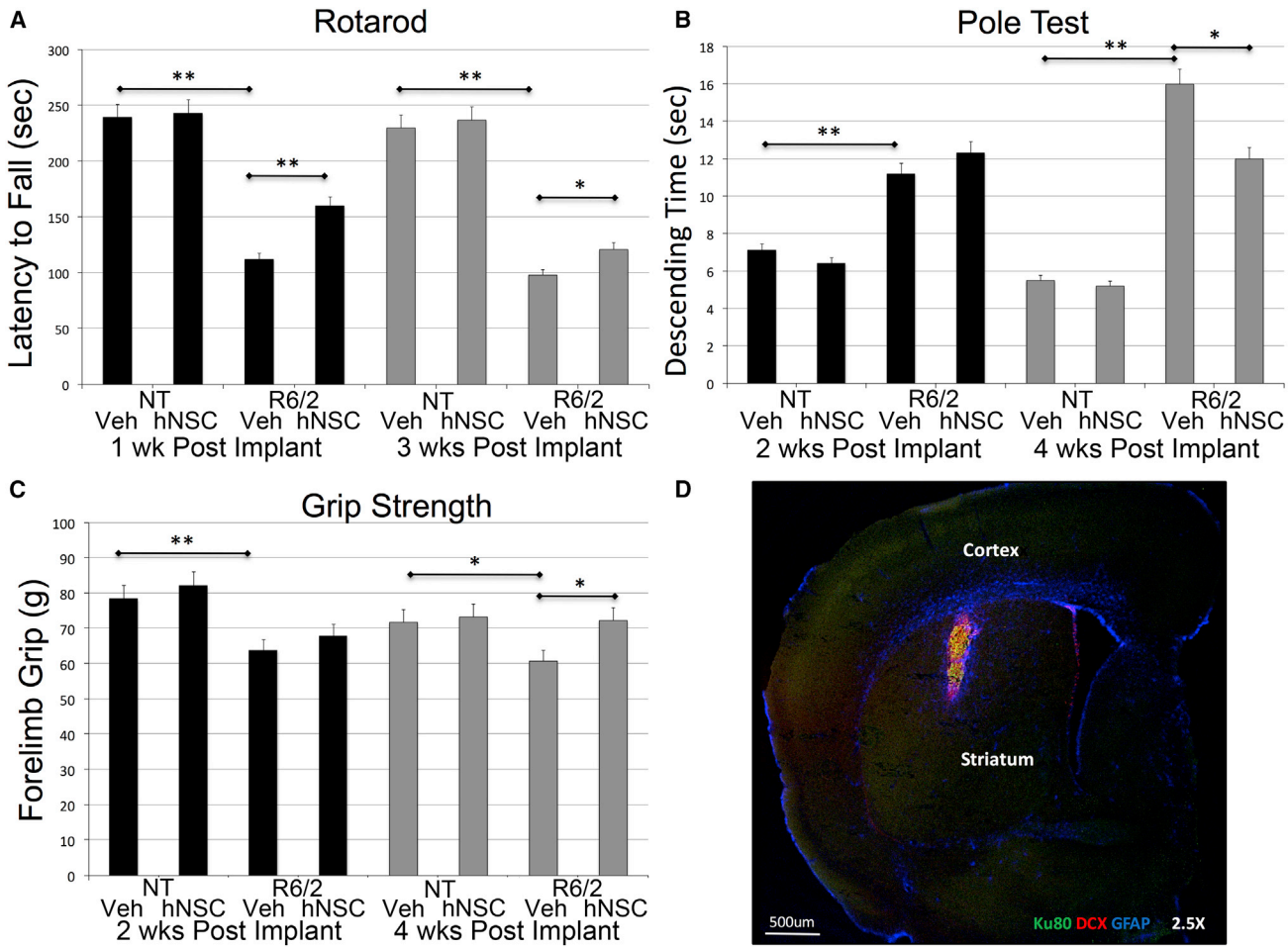

Figure 1. ESI-017 hNSCs Implanted in R6/2 Mice Improve Behavior and Exhibit Evidence of Differentiation into Immature Neurons and Astrocytes

(A) Rotarod task demonstrates a deficit in R6/2 mice compared with non-transgenic littermates (NT), and hNSC-treated R6/2 mice have increased average latency to fall 1 week (black bars) and 3 weeks (gray bars) after implantation compared with vehicle-treated (Veh) mice.

(B) Pole test demonstrates a deficit with R6/2 mice compared with NT. hNSC-treated R6/2 mice descend faster than Veh mice 4 weeks after implantation (gray bars) but not 2 weeks after implantation (black bars).

(C) Grip strength demonstrates a deficit in R6/2 mice compared with NT. hNSC-treated R6/2 mice have greater grams of strength after 4 weeks compared with Veh mice (black bars) but not after 2 weeks (gray bars).

(D) Immunohistochemistry (IHC). hNSCs (human marker SC121, green) implanted in striatum of R6/2 mice co-localize (yellow) with marker for neuron-restricted progenitors (doublecortin [DCX], red) and astrocytes (SC121 and GFAP, blue).

One-way ANOVA followed by Tukey's HSD test with Scheffé, Bonferroni, and Holm multiple comparison calculation performed post hoc. *$p < 0.05$, **$p < 0.01$ ($n = 15$). Graphs show means ± SEM.

membrane capacitance than host MSNs (hNSC 22.0 ± 1.8 pF, n = 31 versus MSN 71.3 ± 3.5 pF, n = 44; $p < 0.001$, Student's t test) and a significantly higher membrane input resistance (hNSC 2804.8 ± 203.0 MΩ versus MSN 163.8 ± 15.1 MΩ; $p < 0.001$, Student's t test). hNSCs showed spontaneous excitatory and inhibitory postsynaptic currents (sEPSCs and sIPSCs), indicating that they received synaptic inputs from the host tissue or other implanted hNSCs. However, compared with MSNs, frequencies were much lower. Some hNSCs also generated action potentials spontaneously, suggesting that they could affect host neurons and neighboring hNSCs (Figure 3B).

Electrophysiological alterations occur in MSNs from symptomatic R6/2 compared with NT mice, including changes in intrinsic membrane properties and reduced excitatory synaptic activity (Cepeda et al., 2003, 2007). hNSC implantation did not significantly alter membrane properties, average sEPSC frequency (1.1 ± 0.1 Hz versus

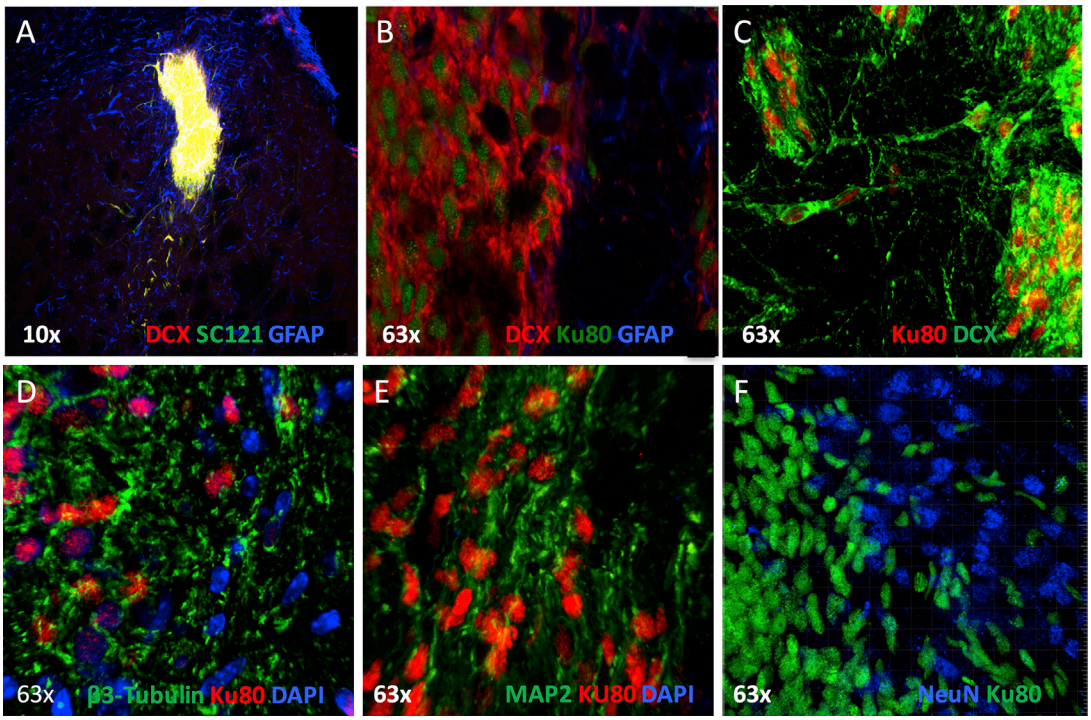

Figure 2. IHC Shows that ESI-017 hNSCs Implanted in R6/2 Mice Differentiate

(A) hNSCs (SC121, green) implanted in R6/2 mice differentiate into neuron-restricted progenitors (doublecortin [DCX], red) and astrocytes (SC121 and GFAP, blue).

(B) High magnification (63×) showing differentiation: hNSCs (human nuclear marker Ku80, green) implanted in R6/2 mice differentiate into neuron-restricted progenitors (DCX, red) and some astrocytes (Ku80 and GFAP, blue).

(C) hNSCs (Ku80, red) and neuron-restricted progenitors (DCX, green).

(D) hNSCs (Ku80, red) and neuron-restricted progenitors (βIII-tubulin, green); mouse cell nuclei shown with DAPI in blue.

(E) hNSCs (Ku80, red) and neuron-restricted progenitors (MAP-2, green); mouse cell nuclei shown with DAPI in blue.

(F) hNSCs (Ku80, green) do not co-localize with differentiated post-mitotic neuronal cell marker (NeuN, blue).

1.4 ± 0.2 Hz) or average sIPSC frequency of MSNs in R6/2 mice. R6/2 mice also display an increase in cortical pyramidal cell excitability and a propensity to develop epileptic discharges and seizures (Cummings et al., 2009). Cortical hyperexcitability is shown in striatal MSNs by the occurrence of large-amplitude EPSCs and high-frequency bursts, particularly evident after extended blockade of $GABA_A$ receptors coinciding with an increase in the frequency of sEPSCs (Cepeda et al., 2003; Cummings et al., 2009). A smaller proportion (not statistically significant) of MSNs exhibited increased corticostriatal excitability in hNSC-implanted mice (20.5%, 9/44) compared with veh mice (28.6%, 16/56). However, the increase in sEPSC frequencies within this population did not occur in the R6/2 mice implanted with hNSCs. A rightward shift in the cumulative probability distribution of the inter-event interval plot occurred ($p < 0.001$), indicating that the hNSCs can reduce hyperexcitable input from cortex to striatum when $GABA_A$ receptors are blocked (Figures 3E and 3F).

Host Tissue Makes Potential Synaptic Contacts with Implanted ESI-017 hNSCs in R6/2 Mice

We utilized immunohistochemistry (IHC) and electron microscopy (EM) to examine whether nerve terminals from the host make synaptic contact with the hNSCs. We find examples of unlabeled nerve terminals originating from the host making a potential symmetrical synaptic contact with the implanted and immunolabeled hNSCs (Figure 4A). A few synaptic vesicles within the nerve terminal are very close to the presynaptic membrane, indicating a potential area of vesicular release (DAB labeling of hNSCs is obscuring contact). In addition, we found unlabeled nerve terminals originating from the host making a clearly asymmetrical contact (Figure 4B), suggesting an excitatory synaptic contact. Overall, we find that of the unlabeled nerve terminals originating from the host, 44.5% (n = 71) were making an asymmetrical contact while 48.3% (n = 69) were making symmetrical contacts with the labeled hNSCs. Of the remaining 7.2% (n = 11) of unlabeled nerve terminals originating

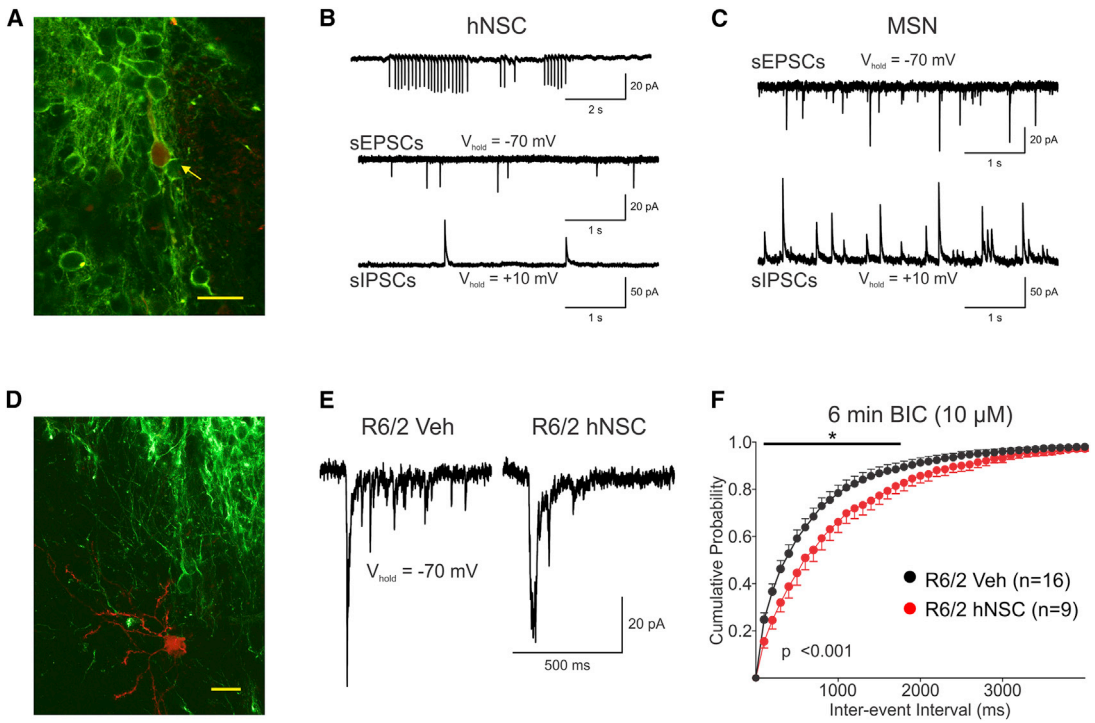

Figure 3. Implantation of ESI-017 hNSCs Reduces Corticostriatal Hyperexcitability in R6/2 Mice

(A) Biocytin-filled (red, yellow arrow) hNSC that was recorded in the striatum and IHC with SC121 (green). Scale bar, 20 μm.

(B) Top trace: cell-attached recording of spontaneously firing hNSC. Bottom traces: sEPSCs and sIPSCs from hNSC. Recordings illustrate spontaneous inward and outward synaptic currents in the hNSC.

(C) sEPSCs and sIPSCs recorded in MSN.

(D) Biocytin-filled MSN (red) near a cluster of hNSCs (SC121 green). Scale bar, 20 μm.

(E) Recordings of sEPSCs in a subpopulation of R6/2 MSNs show "epileptiform" activity after the addition of the $GABA_A$ receptor antagonist, bicuculline (10 μM) (first trace). These large-amplitude excitatory events are usually followed by high-frequency small-amplitude sEPSCs. In mice with hNSC implants these events were markedly reduced in frequency (second trace).

(F) In cells with "epileptiform" activity (6–8 min after BIC), there was a rightward shift in the cumulative inter-event interval probability distributions for the hNSC-implanted R6/2 group compared with vehicle, corresponding to a significant decrease in high-frequency spontaneous events ($p < 0.001$, two-way repeated-measures ANOVA followed by Bonferroni post hoc analysis; $^*p < 0.05$).

from the host juxtaposed to the labeled hNSCs, the exact nature of their contact (asymmetrical versus symmetrical) could not be determined.

ESI-017 hNSCs Rescue Behavior, Survive, and Differentiate in Q140 Knockin Mice

We next determined whether hNSCs could also improve deficits in a slowly progressing full-length HD mouse model. Q140 mice express a modified mouse/human exon 1 with ~140 repeats inserted into the mouse huntingtin gene (Menalled et al., 2003). Homozygous mice exhibit early abnormalities in motor tests with climbing deficits at age 1.5 months, and cognitive deficits (Hickey et al., 2008; Simmons et al., 2009) and visible aggregates of HTT around 4 months (Menalled et al., 2003). Striatal atrophy is detected at 1 year with a 35% striatal cell loss at 22 months (Hickey et al., 2008). Twenty-four 2-month-old homozygous male and female mice per group were dosed with 100,000 hNSCs per hemisphere, stereotactically delivered bilaterally into the striatum (n = 12/sex) with control age-matched Q140 (n = 12/sex) and wild-type (WT) (n = 12/sex) mice injected with veh. All mice were immunosuppressed. Behavior testing began at age 1.5 months (before cell transplantation) and mice were euthanized at 8 months, 6 months after transplantation. Behavioral tests were performed on all mice except for the running wheel, where only males were used since estrus cycle influences running activity (Hickey et al., 2008). Early deficits in locomotor activity in the open field as well as decrease in spontaneous motor activity in the climbing cage test were observed in Q140 mice; however, hNSC treatment did not rescue performance (Figure S4).

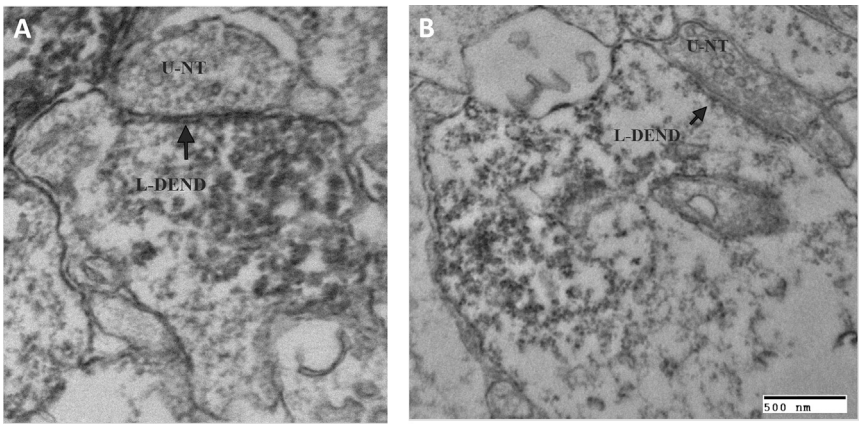

Figure 4. Nerve Terminals from the Host Make Synaptic Contact with the Implanted hNSCs

(A) Unlabeled nerve terminal (U-NT), containing synaptic vesicles, making a synaptic-like contact (arrow) with an underlying labeled (SC121) hNSC dendrite (L-DEND). The connection may be symmetrical.

(B) Unlabeled nerve terminal (U-NT), containing synaptic vesicles, making an asymmetrical synaptic contact (arrow) with an underlying labeled (SC121) hNSC dendrite (L-DEND). This asymmetrical contact suggests an excitatory synaptic contact.

In pole tests veh-treated Q140 mice took longer to turn compared with WT controls ($p = 0.004$); in contrast, hNSC-treated Q140 mice were significantly better than control Q140 mice ($p = 0.04$) and no longer significantly different from WT, indicating a beneficial effect 3 months post transplantation (Figure 5A). As reported by Hickey et al. (2008), 5.5-month-old male Q140 mice had profound deficits in running speed (rotations per 3 min), significant for 2 weeks (Figure 5B). Persistent improvement of running wheel deficits was observed post treatment with hNSC-treated Q140 mice, showing a progressive increase in average running wheel activity compared with veh-treated mice (Figures 5B and 5C). We conclude that hNSC administration improved some of the motor deficits observed in Q140 mice.

Novel object recognition (NOR) is a cortical-dependent cognitive test that requires both learning and memory (recognition) and takes advantage of the tendency of mice to investigate a novel object over a familiar one. Veh-injected Q140 mice exhibited significant impairments in NOR compared with veh-injected WT mice at 3 and 5 months post implant ($p = 0.003$ and $p = 0.03$, respectively) as reported by Simmons et al. (2009). Striatal transplantation of hNSCs in Q140 mice rescued cognitive impairments at 5 months post implant ($p = 0.03$), but not earlier (Figures 5E and 5F).

A subset ($n = 5$ for each group) of veh- and hNSC-transplanted Q140 male mice were euthanized at 6 months post treatment for IHC analyses. hNSCs, identified with a human nuclear-specific antibody (HNA), were present 6 months post transplantation and mostly confined to the injection tract (Figure 5Ga,b) in the striatum. The number of HNA-positive cells counted over the entire striatal area in six coronal sections and cells double-labeled with DCX or GFAP was calculated (mean data from 5 mice per group ± SEM). Approximately 25% of the 100,000 hNSCs survive with most (84% ± 2%) being GFAP positive (Figure 5Gb,c), a smaller proportion (16% ± 2%) being DCX positive (Figure 5Ge,f).

ESI-017 hNSC Transplantation Increases BDNF Levels in HD Mice

Increased levels of neurotrophic growth factors and subsequent increased synaptic connectivity are implicated in behavioral ameliorations observed after transplantation of NSCs (Blurton-Jones et al., 2009). Furthermore, reduced BDNF has been demonstrated for multiple mouse models of HD and in human HD brain (Zuccato et al., 2011). Therefore, we evaluated BDNF levels as a marker for neurotrophic effects. In the R6/2 hNSC mice, IHC and confocal microscopy indicated co-localization of BDNF with DCX-positive hNSCs, suggesting that the differentiated cells produce BDNF (Figure 6A). Indeed, hNSCs grown *in vitro* and differentiated produce BDNF only after becoming DCX positive (Figure S5). In the Q140 hNSC mice, BDNF was quantified by ELISA in a subset of male mice ($n = 6$/group). Striatal BDNF was decreased in Q140 mice compared with WT, but a significant increase in BDNF levels was observed in hNSC-treated compared with veh, restoring it to WT levels (Figure 6C).

Given that neurotrophic signaling can enhance synaptic activity, we examined levels of synaptophysin, a synaptic marker, in the striatum of all perfused Q140 animals ($n = 5$/group) by IHC and quantification using a microarray scanner as previously described (Richter et al., 2017). Comparison of hNSC- with veh-treated Q140 mice revealed a significant increase in synaptophysin in the hNSC mice (Figure S6A, quantified in Figure S6B).

These results suggest that engrafted hNSCs may in part improve synaptic connectivity by increased neurotrophic effects, including BDNF.

ESI-017 hNSC Treatment in Q140 Mice Decreased Microglial Activation

Striatal sections from Q140 mice ($n = 5$/group) were stained with an Ionized calcium-binding adaptor molecule 1 (Iba-1) antibody which identifies both resting and reactive microglia. Microglial soma sizes correlate with activation

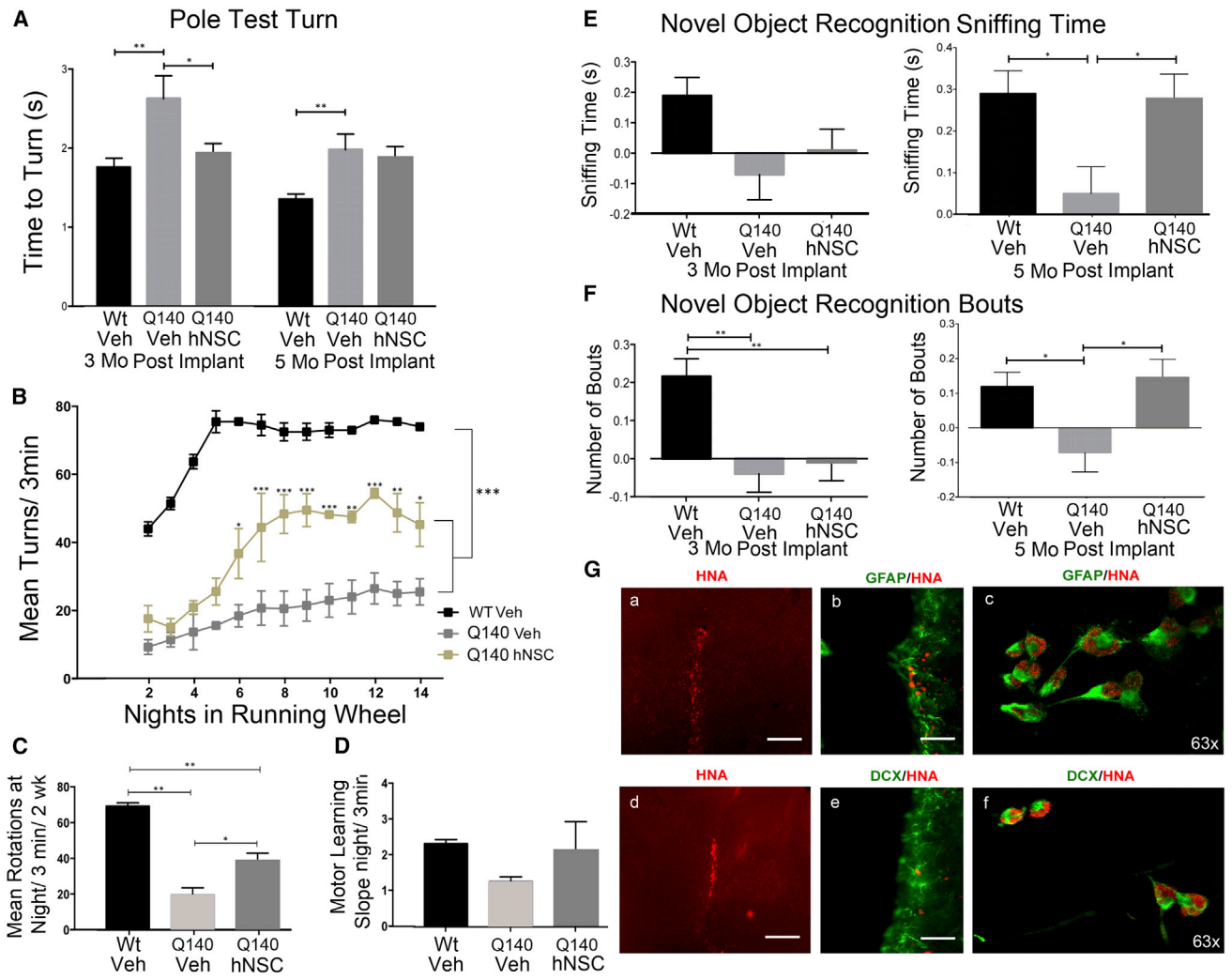

Figure 5. ESI-017 hNSCs Implanted in Q140 Mice Improve Behavior and Exhibit Evidence of Differentiation into Immature Neurons and Astrocytes

(A) Transient improvement in motor coordination (pole task) 3 months after cell injection. WT Veh (n = 20), Q140 Veh (n = 18), Q140 hNSC (n = 18). One-way ANOVA with Bonferroni post hoc test: *p < 0.05, **p < 0.01.

(B–D) Persistent improvement of running wheel deficits 5.5 months post treatment (n = 5 per group). (B) Graph showing mean running wheel rotations/3 min/night over 2 weeks, in 7.5-month-old male WT or Q140 mice 5.5 months post treatment. Comparison by two-way ANOVA: group effect F = 52.93, p < 0.0001; night in running wheel effect F = 17, p < 0.0001. Bonferroni post hoc test: *p < 0.01, **p < 0.001, and ***p < 0.0001 compared with Q140 Veh. (C) Total average running wheel turns at night over 2 weeks. Two-way ANOVA with Bonferroni post hoc test: *p < 0.01, **p < 0.001. (D) Slope of motor learning not significant between the three groups.

(E and F) Novel object recognition. hNSCs prevented the deficit in Q140 mice 5 months post treatment but not at 3 months in the discrimination index of sniffing time (E) or number of bouts (F). WT Veh n = 18, Q140 Veh n = 18, and Q140 hNSC n = 19. One-way ANOVA with Bonferroni post hoc test: *p < 0.05, **p < 0.01.

(G) Survival and differentiation of hNSCs in Q140 mice by staining with the human specific antibody (HNA, red; a and d) co-expressing with astrocytes (GFAP, green; b and c) or neuron-restricted progenitors (DCX, green; e and f). Scale bar, 20 μm.

All graphs show mean ± SEM.

state cell morphology (Watson et al., 2012) and a significant increase in the diameter of Iba1-positive cells (strong microglial response) was observed in the striatum of Q140 mice. This response was significantly reduced by hNSCs (Figure 6D). Similar analysis in hNSC-implanted R6/2 mice did not show a significant alteration in the

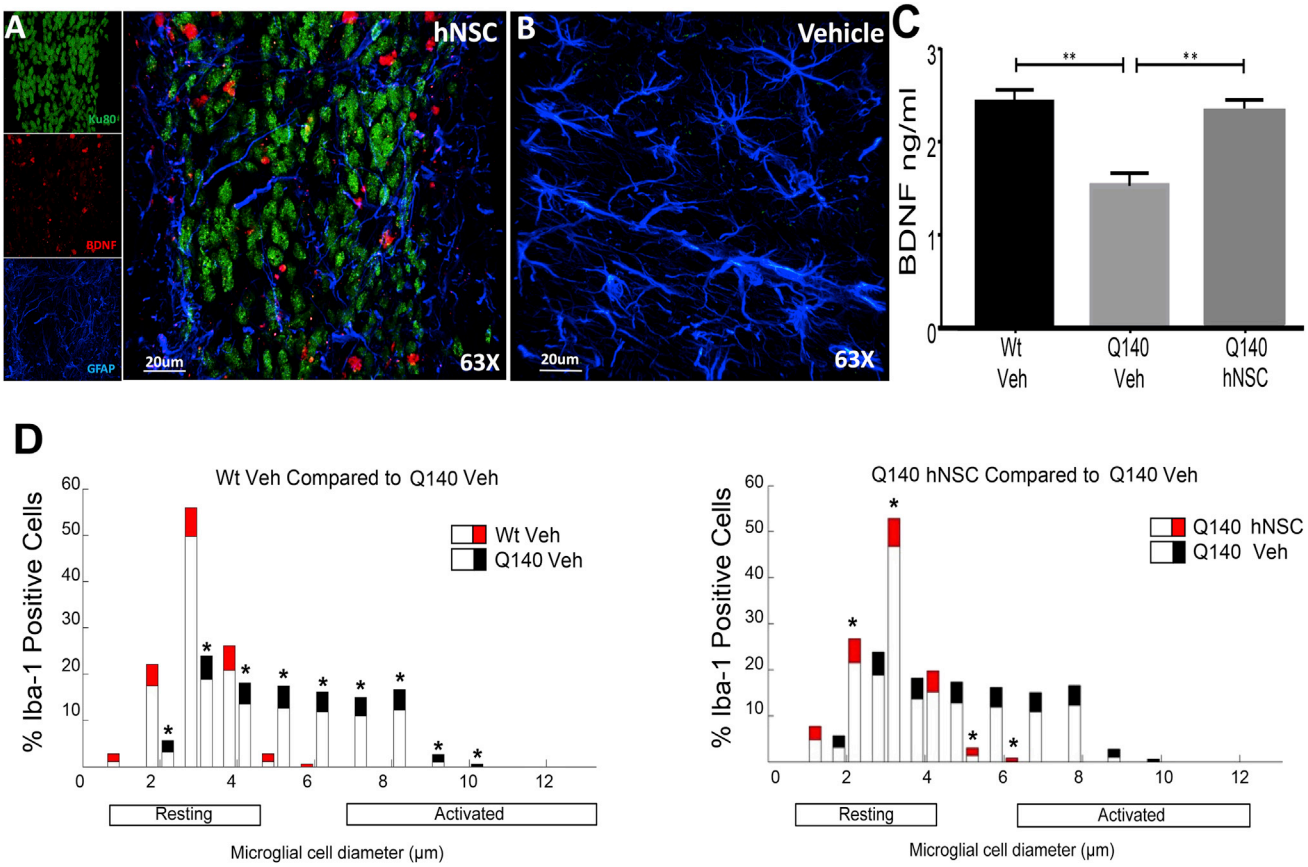

Figure 6. ESI-017 hNSCs Implanted in HD Mice Increase Expression of BDNF

(A) ESI-017 hNSCs (Ku80, green) show co-localization with BDNF (red); astrocytes are shown as GFAP positive (blue).

(B) Veh-treated mice show no BDNF or hNSCs but have GFAP (blue).

(C) BDNF levels by ELISA in striatum of Q140 or WT mice 6 months post implant.

(D) hNSC treatment in Q140 mice decreased microglial activation. Data are presented as the mean + 95% confidence interval (n = 5 per group). Bars represent percentage of cells of each diameter and the colored portion represents the confidence interval. Significant striatal microglial activation observed in Q140 Veh compared with WT Veh. Q140 hNSC mice showed significant reduction of microglial activation in striatum compared with Q140 Veh mice.

*$p < 0.05$ and **$p < 0.01$ by one-way ANOVA with Bonferroni post hoc test. Graphs show means ± SEM.

striatum (Figure S6) and may be due to a relatively localized effect or a moderate level of activated microglia.

ESI-017 hNSC Transplantation Reduces mHTT Accumulation and Aggregates

A hallmark of HD pathology is the presence of HTT inclusions that may reflect altered protein homeostasis. Therefore, we performed unbiased stereological assessments on brain sections from R6/2 and Q140 mice. For R6/2 mice, sections were stained first for Ku80 with nickel-enhanced DAB (black), then for HTT (EM48) using DAB without nickel, then with cresyl violet counterstain for non-hNSC nuclear staining. Figure 7A shows the area where stereology was performed adjacent to the hNSC implant; areas away from the implant did not show significant differences in mutant HTT (mHTT) accumulation or aggregates. Results indicate that R6/2 mice implanted with hNSCs have decreased diffuse staining and decreased inclusion numbers near the injection site compared with veh (Figures 7A and 7B).

A clear decrease in aggregate numbers was also observed in the striatum of Q140 mice (Figure 7C). At 6 months post treatment, hNSC-treated Q140 mice had fewer diffusely stained nuclei ($p = 0.0102$) and fewer neuropil aggregates ($p = 0.0239$), but no reduction in nuclear inclusions nor microaggregates ($p = 0.0753$ and $p = 0.372$, respectively) compared with veh-treated mice (Figure 7D). This result suggests that hNSC delivery modulated HD-related pathology. No acquisition of inclusions was observed in or near transplanted cells in either R6/2 (Figure S3D) or Q140 mice.

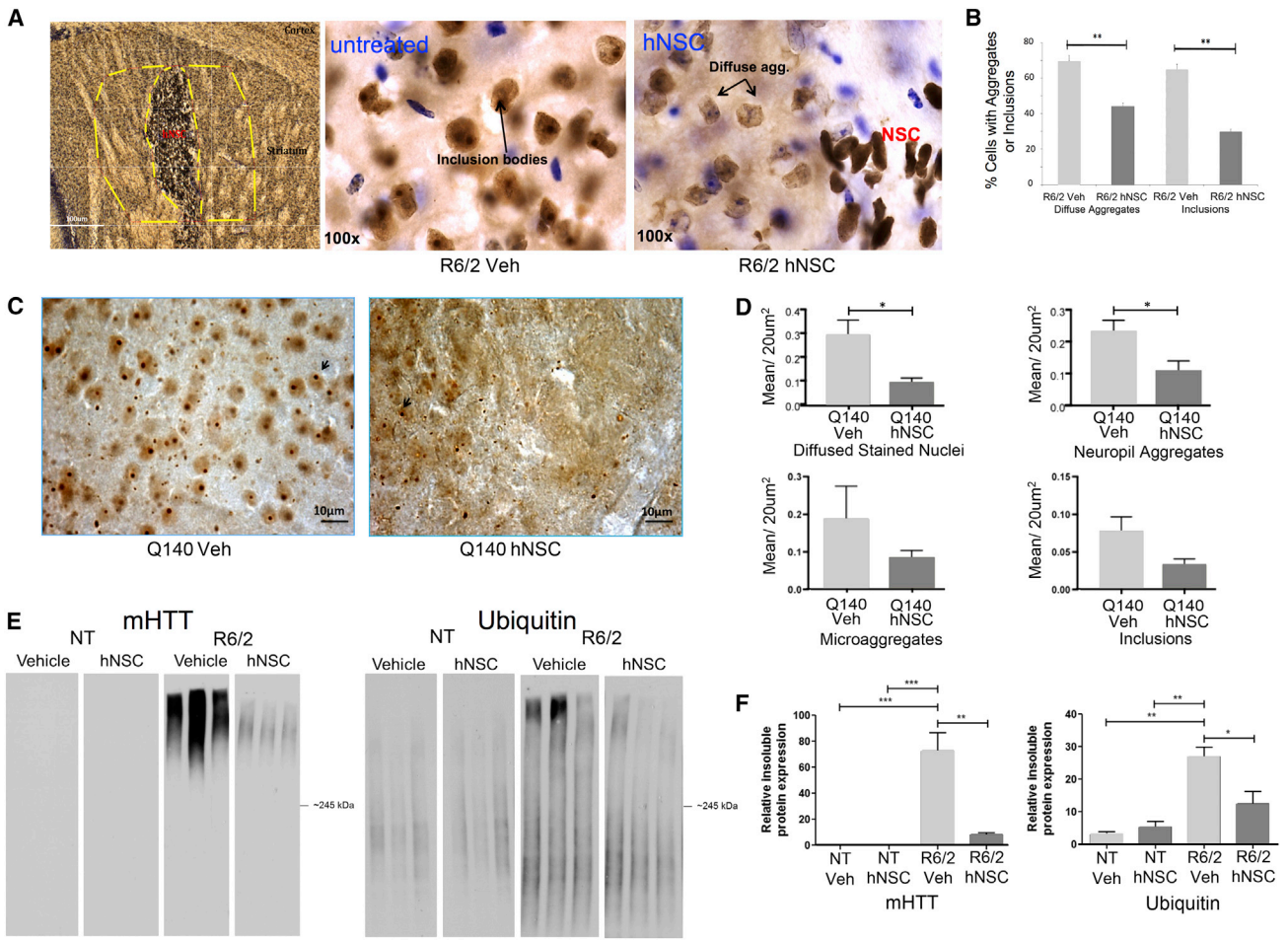

Figure 7. ESI-017 hNSCs Implanted in R6/2 Mice Cause Decreases in Diffuse Aggregates and Inclusions and Reduce Huntingtin Aggregates in Q140 Mice

(A and B) ESI-017 hNSCs cause decreases in diffuse aggregates and inclusions (arrows in A) in R6/2 mice. (A) Image of Ku80 with nickel, HTT marker EM48, and cresyl violet for non-hNSC nuclear staining. Stereological assessment performed using StereoInvestigator. Contour tracing under 5× objective (dashed lines, example in left panel) and counting at 100×. Every third section was counted (40-µm coronal sections) for 6 sections throughout the striatum where Ku80 could be seen between bregma 0.5 mm and bregma −0.34 mm. (B) Graph depicting percentage of cells with aggregates or inclusions (n = 4/group) $^{**}p < 0.01$ by one-way ANOVA with Bonferroni post hoc test. (C and D) ESI-017 hNSCs reduce Huntingtin aggregates in Q140 mice. (C) Images of HTT marker EM48 (arrows indicate inclusions). (D) HTT-stained nuclei and aggregates were analyzed with StereoInvestigator for quantification of aggregate type/section. Data are shown as mean ± SEM (n = 5/group). $^{*}p < 0.05$ by one-way ANOVA with Bonferroni post hoc test.

(E and F) hNSC transplantation modulates insoluble protein accumulation in R6/2 mice. Western blot of striatal lysates separated into detergent-soluble and detergent-insoluble fractions. (E) R6/2 enriched in insoluble accumulated mHTT compared with NT. hNSC transplantation in R6/2 results in a significant reduction of insoluble HMW accumulated HTT compared with veh-treated animals. R6/2 striatum is also enriched in insoluble ubiquitin-conjugated proteins compared with NT. hNSC transplantation in R6/2 mice results in a significant reduction of ubiquitin-modified insoluble conjugated proteins compared with veh treatment with no significant effect in NT compared with veh controls. (F) Quantitation of the relative protein expression for mHTT and ubiquitin. Values represent means ± SEM. Statistical significance for relative insoluble accumulated mHTT and ubiquitin-conjugated protein expression in R6/2 was determined with a one-way ANOVA followed by Bonferroni post hoc test (n = 3/treatment). $^{*}p < 0.05$, $^{**}p < 0.01$, $^{***}p < 0.001$. Graphs show means ± SEM.

hNSC Transplantation Decreases Pathogenic Accumulation of mHTT and Ubiquitinated Proteins

We next examined the impact of hNSC treatment on high molecular weight (HMW) mHTT species and ubiquitin-modified proteins that accumulate in R6/2 brain. Reduction of these insoluble proteins corresponds to improved behavioral outcomes in R6/2 mice (Ochaba et al., 2016). Evaluation of a detergent-insoluble fraction of NT and

R6/2 striatum with and without hNSC transplantation indicated that accumulated mHTT levels were significantly increased in R6/2 striatum, and treatment with hNSCs decreased insoluble HTT accumulation by ~70% in R6/2 striatum compared with veh-treated mice (Figures 7E and 7F), which was not due to altered mHTT transgene mRNA expression (Figure S7). Accumulated ubiquitin-conjugated proteins were also significantly increased in R6/2 striatum compared with NT mice and hNSC treatment decreased insoluble ubiquitin-conjugated proteins in R6/2 mouse striatum compared with veh-treated mice (Figures 7E and 7F). No significant difference was detected in treated NT mice.

DISCUSSION

Stem cell-based transplantation strategies are promising approaches for neurodegenerative disorders based on their ability to modulate pathology through regenerative and restorative mechanisms. In HD models, mouse-derived NSCs have shown promising results while hNSC-based approaches have had mixed success, with robust efficacy in toxin models and limited neuroprotection in genetic HD mice (El-Akabawy et al., 2012; Golas and Sander, 2016). Here we describe transplantation of GMP-grade hNSCs that provides robust rescue of deficits and disease-modifying activity targeting the accumulation of the mHTT protein. ESI-017 hNSCs were electrophysiologically active in R6/2 mice but did not have significant effects on striatal MSN membrane properties or spontaneous synaptic activity. In a subset of MSNs, however, the increase in frequency of sEPSCs commonly observed after extended blockade of $GABA_A$ receptors with bicuculline did not occur, suggesting that the grafts help to reduce cortical hyperexcitability. We have not determined the underlying mechanisms of this effect, but electrical stimulation inside the graft induces IPSCs in neighboring cells, suggesting that they are inhibitory. The ultrastructural data show that the host is potentially making both symmetrical (inhibitory) and asymmetrical (excitatory) synaptic contacts in equal numbers with the hNSCs. Our assumption is that the effects are derived from the implanted cells and that in R6/2 mice they are primarily differentiating along a neuronal lineage. However, in other experiments including the Q140 mice, there is a potential glial effect, suggesting that the driver of improvement is not yet understood. Given that neuronal loss does not occur in these mice until very late stages of disease, the striatal-specific transplantation appears to act through both neuroprotection via trophic factors such as BDNF and by preventing the aberrant accumulation of mHTT species. However, the finding of electrophysiological activity in transplanted cells, and contact between human and endogenous mouse cells that may facilitate improved electrophysiological outcomes, suggest that there may also be an opportunity for regenerative effects.

The rationale for transplanting NSCs versus other progenitor types is based on their ability to differentiate along multiple lineages. In R6/2 mice, cells exhibited evidence of early astrocytic or neuronal differentiation; most co-label with neuron-restricted progenitor markers (DCX, βIII-tubulin, and MAP-2). As hNSCs typically take several months to terminally differentiate, we expected to observe only partial differentiation of transplanted cells at the 4-week time point. Interestingly, very few ESI-017 hNSCs are DCX positive before implantation *in vitro*. Results of cell fate in R6/2 mice are in contrast to our findings in the Q140 long-term HD model and other studies in Parkinson's disease and Alzheimer's disease (AD) models using hNSCs where more cells are becoming astrocytes (Goldberg et al., 2017), although the latter are derived from fetal NSCs, which tend to be more gliogenic. These data suggest that there may be different responses depending on the disease niche, immunosuppression paradigms may influence specification, or developmental cues and timing specific to human versus mouse cells influences outcomes.

Diminished BDNF levels are present in HD mice and in human HD subjects (Strand et al., 2007; Zuccato et al., 2011), and many efficacious treatments in HD mice show a concomitant increase in BDNF (Ross and Tabrizi, 2011). Consistent with the idea of trophic factor support through stem cell transplantation; *ex vivo* delivery of mouse NSCs expressing GDNF maintains motor function and prevents neuronal loss in HD mice (Ebert et al., 2010), and BDNF was required for improved cognition following mouse NSC transplantation into either AD mice (Blurton-Jones et al., 2009) or a model of dementia with Lewy bodies (Goldberg et al., 2015). BDNF must be trafficked to the striatum via the afferent pathways, including the corticostriatal pathway that is altered in HD (Laforet et al., 2001). It is possible that by supplying trophic support to the striatum, the corticostriatal pathway is preserved enough to signal BDNF production in the cortex or that stem cell-derived BDNF is retrogradely transported from the striatum back to the soma of corticostriatal neurons, leading to improved electrophysiological activity following transplantation.

One mechanism of action of implanted hNSCs may be via reduction of aberrant mHTT accumulation and aggregates, potentially through preventing their formation or inducing selective clearance mechanisms (e.g., Chen et al., 2013). We recently described findings that reduction of a specific HMW insoluble mHTT species was associated with improved behavior and normalization of several molecular readouts in R6/2 mice (Ochaba et al., 2016). It is plausible that reduction of pathogenic accumulation of mHTT and ubiquitinated HMW insoluble species

prevents the neuronal dysfunction that is observed in the HD mice.

It is important to note that in contrast to the observation that aggregates could be acquired in a study of fetal cell transplants in human HD subjects (Cicchetti et al., 2014), no evidence of acquired HD phenotypes, such as inclusions, were observed over the course of the transplants in either mouse model (Figure S3). The lack of apparent protein propagation or acquired pathology could be a result of increased trophic signaling of the hNSCs or from reducing mHTT species that could otherwise facilitate protein propagation into the transplanted cells. Alternatively, it could take years for the cells to acquire pathology, which is not represented by the mouse studies.

In summary, we show that hNSCs transplanted into HD mice survived, differentiated into neural populations, may protect or repair damaged tissue and delay disease progression, decreased pathologies and increased production of protective molecules, and potentially formed contacts with surrounding tissue, suggesting a prospective treatment strategy for HD. Given the results by An et al. (2012) showing that genetically corrected patient-derived NSCs can form human neurons and DARPP-32-positive cells and the results reported here, future application of autologous transplantation using corrected patient cells may also be feasible.

EXPERIMENTAL PROCEDURES

Mice

All procedures were in accordance with Guide for the Care and Use of Laboratory Animals of the NIH and approved animal research protocols by Institutional Animal Care and Use Committees at UCI and UCLA, AAALAC accredited institutions. R6/2 mice and their NT littermates (Transgene non-carrier C57Bl6/CBA) were obtained from breeding colonies maintained at UCI (line 6494, ~120 ± 5 CAG repeats) or UCLA (line 2810, ~150 ± 5 CAG repeats). Homozygous Q140 mice or WT (C57Bl6) littermates were from breeding colonies at UCLA, where procedures were performed. All mice were housed on 12/12-hr light/dark schedule with *ad libitum* access to food and water. Mice were group housed as mixed treatment groups and only singly housed for the running wheel. CAG repeat length was confirmed for R6/2 mice (Laragen, Los Angeles, CA), and for Q140 mice frequency distributions are not significantly different (Hickey et al., 2012b). Assessment of differences in outcome were based upon previous experience and published results (Hickey et al., 2005; Hockly et al., 2003) for HD models, and applying power analysis (G Power [http://www.psycho.uni-duesseldorf.de/abteilungen/aap/gpower3/]) led us to a minimal n = 10 for behavior and n = 4 for biochemical analysis.

hNSC Isolation

The use of hNSCs was approved by UCI's, UCLA's, and UC Davis' Human Stem Cell Research Oversight Committee (hSCRO) and cells were derived from Biotime ESI-017 hESCs. hESC colonies were transferred to EB medium with Noggin, transitioned to NP medium, and the rosettes dissected out, dissociated, and plated down with hNSC medium to generate hNSCs (Figure S1B). Rosettes were manually dissected out and plated into growth factor-reduced Matrigel-coated plates in NSC medium then dissociated using Accutase and plated onto polyornithine/laminin-coated plates with NSC medium. Daily culturing is described in detail in Supplemental Experimental Procedures.

Transplantation Surgery

Bilateral intrastriatal injections of hNSCs or veh were performed using a stereotactic apparatus and coordinates relative to bregma: anteroposterior, 0.00; mediolateral, ±2.00; dorsoventral, −3.25. Mice were anesthetized, placed in the stereotactic frame, and injected with either 100,000 hNSCs/side (2 μL/injection) or veh (2 μL Hank's balanced salt solution with 20 ng/mL human epidermal growth factor [STEMCELL Technologies, #78003] and human fibroblast growth factor [STEMCELL, #78006]) using a 5-μL Hamilton microsyringe (33-gauge) and injection rate 0.5 μL/min. Wounds were sealed and the mice recovered in cages with heating pads. Immunosuppressants were administered the day before surgeries to all mice and continued throughout. Specific details are provided in Supplemental Experimental Procedures.

Behavioral Assessment

R6/2

Mice were assigned in a semi-randomized manner and behavioral tests performed between 6 and 9 weeks. Researchers were blind to genotype and treatment for testing and data collection. To minimize experimenter variability, a single investigator conducted each test. Behavior tasks in R6/2 mice were performed as previously described by Ochaba et al. (2016) and in Supplemental Experimental Procedures.

Q140

Males and females were used except for the running wheel, where only males were used since estrus cycle influences running activity. Genotypes or treatments were unknown to the experimenter. All tests were done during the light phase except for the running wheel, conducted during the dark phase. Behavior tasks in Q140 mice were performed as previously described by Hickey et al. (2008) and in Supplemental Experimental Procedures.

Electrophysiology in R6/2 Brain Slices

R6/2 (line 2810, 150 ± 10 CAG repeats) and NT littermates were used, expressing a phenotype similar to that of the 6494 line used for behavioral experiments (Cummings et al., 2012). Procedures were as described by Andre et al. (2011) with modifications as detailed in Supplemental Experimental Procedures.

Immunohistochemistry and Electron Microscopy

Male R6/2 mice implanted with hNSCs for 5 weeks (n = 3) were anesthetized and perfused with EM fixative (2.5% glutaraldehyde, 0.5% paraformaldehyde, and 0.1% picric acid in 0.1 M phosphate buffer [pH 7.4]). Brains were then collected into EM fixative overnight at 4°C and washed in PBS until serially sectioning through

striatum containing hNSCs (equivalent to +1.4 to +0.14 mm from bregma) (Franklin and Paxinos, 2007) at 60 μm using a vibratome (Leica Microsystems). Pre-embed IHC of striatum using diaminobenzidine (DAB) (Sigma, St Louis, MO) and hNSC antibody (Stem121, 1:100; StemCells) tissue processed for EM was as previously described (Spinelli et al., 2014; Walker et al., 2012), and striatum slices were embedded flat between two sheets of ACLAR (Electron Microscopy Sciences, Hatfield, PA) overnight in a 60°C oven to polymerize resin. The area containing hNSCs was microdissected from the embedded slice and superglued onto a block for thin sectioning.

Photographs were taken on a JEOL 1400 transmission electron microscope (JEOL, Peabody, MA) of DAB-labeled structures (i.e., hNSC-labeled cells, dendrites) at a final magnification of ×46,200 using a digital camera (AMT, Danvers, MA). Since the DAB labeling was restricted to the leading edge of the thin-sectioned tissue, only the area showing DAB labeling was photographed.

Biochemical, Molecular, and Immunohistological Analysis in R6/2 Mice

Mice were euthanized by pentobarbital overdose and perfused with 0.01 M PBS. Striatum and cortex were dissected out of the left hemisphere and flash frozen for RNA, and protein isolated in TRIzol using the manufacturer's procedures (Life Technologies, Grand Island, NY) or homogenized as described below. The other halves were post-fixed in 4% paraformaldehyde, cryoprotected in 30% sucrose, and cut at 40 μm on a sliding vibratome for IHC. Sections were rinsed three times and placed in blocking buffer for 1 hr (PBS, 0.02% Triton X-100, 5% goat serum), and primary antibodies placed in block overnight (ON) at 4°C. Sections were rinsed, incubated for 1 hr in Alexa Fluor secondaries, and mounted using Fluoromount G (Southern Biotechnology). Primary antibodies are listed in Supplemental Experimental Procedures.

Soluble/Insoluble Fractionation

Striatal tissue was processed as described previously (Ochaba et al., 2016). Antibodies: Anti-HTT (Millipore, #MAB5492; RRID: AB_347723) and anti-ubiquitin (Santa Cruz Biotechnology, #sc-8017; RRID: AB_628423). Quantification of bands was performed using software from the NIH program ImageJ and densitometry application.

Confocal Microscopy and Quantification

Sections were imaged with Bio-Rad Radiance 2100 confocal system using lambda-strobing mode. Images represent either single confocal z slices or z stacks. All unbiased stereological assessments were performed using StereoInvestigator software (MicroBrightField, Williston, VT). An optical fractionator probe was used to estimate mean cell, diffuse aggregate, and inclusion body numbers. More details are provided in Supplemental Experimental Procedures.

RNA Isolation and Real-Time qPCR

Striata were homogenized in TRIzol (Invitrogen), followed by RNEasy Mini kit (Qiagen). RIN values were >9 for each sample (Agilent Bioanalyzer). RT used oligo(dT) primers and 1 μg of total RNA with the SuperScript III First-Strand Synthesis System (Invitrogen). qPCR was performed as described by Vashishtha et al. (2013). Primer sequences provided in Supplemental Experimental Procedures.

Biochemical, Molecular, and Immunohistological Analysis in Q140 Mice

Q140 males were euthanized 6 months post treatment by cervical dislocation (n = 7 frozen) or paraformaldehyde perfusion (n = 5 IHC).

IHC

Mice were perfused with 0.1 M PBS and 4% paraformaldehyde. The brains were removed, post-fixed in 4% paraformaldehyde overnight, cryoprotected in 30% sucrose, frozen, and coronal sections cut at 40 μm on a cryostat (Leica CM, 1850). Sections were blocked for 1 hr at room temperature and then primary antibodies used ON. After several washes, sections were incubated in Alexa Fluor secondaries and counterstained with DAPI. IHC for the quantification of HTT aggregates and microglia was performed as described by Menalled et al. (2003) and Watson et al. (2012), respectively. More details are provided in Supplemental Experimental Procedures.

HTT-Stained Nuclei and Aggregates

Sections were analyzed with StereoInvestigator 5.00 software (Microbrightfield, Colchester, VT) (Hickey et al., 2012a). For the contours of striatum drawn, the software laid down a grid of 200 × 200 μm, with counting frames of 20 × 20 μm used for quantification of each type of aggregate per section.

Quantification of IBA-1-Positive Cells in the Striatum of Q140 Mice

Analysis was conducted using a Leica DM-LB microscope with StereoInvestigator software (MicroBrightField) as described for microglial diameter reflecting activation (Watson et al., 2012). For contours of striatum drawn at 5× magnification, the software laid down a grid of 200 × 200 μm, with counting frames of 20 × 20 μm at top left corner allowing for unbiased sampling and quantification.

Biochemical Analysis for Q140 Mice

Frozen striatum processing for ELISAs was performed using a Biosensis BDNF Rapid kit (Biosensis BEK-2211, SA, Australia) as per manufacturer's instructions.

Statistical Analysis

Results for R6/2 mice are from a single cohort except for the electrophysiology and EM data, which were from a different subset; all used the same batch of cells. Numbers were determined to have sufficient power using an analysis prior to the study (described above). Statistical significance was achieved as described using rigorous analysis. All findings are reproducible. Multiple statistical methods are further detailed above, in figure legends, or in Supplemental Experimental Procedures. Significance levels: *$p < 0.05$, **$p < 0.01$, ***$p < 0.001$, ****$p < 0.0001$. In R6/2 mice, data are expressed as mean ± SEM; statistical tests for behavior tasks used one-way ANOVA followed by Tukey's HSD test with Scheffé, Bonferroni, and Holm multiple comparison post hoc. Data met the assumptions of the statistical tests used, and p values less than 0.05 were considered significant. All mice were randomly assigned and tasks performed in a

random manner with individuals blinded to genotypes and treatment. Statistical comparisons of densitometry results were performed by one-way ANOVA followed by Bonferroni's multiple comparison test. Student's t tests were used for aggregate number comparisons from the EM48 stereological study. Significance in clasping was determined by Fisher's exact probability. Statistical analyses for Q140 mice were conducted using GraphPad Prism 6.0 (GraphPad Software, San Diego, CA) for significant differences ($p < 0.05$) in behavioral and postmortem data using one-way ANOVA with Bonferroni post hoc tests. Two-way ANOVA followed by Bonferroni post hoc test was used in the graph representing mean turns in the running wheel/3 min test; and bootstrap statistics using custom MATLAB functions were used for IBA-1 analysis. All error bars on graphs represent SEM.

SUPPLEMENTAL INFORMATION

Supplemental Information includes Supplemental Experimental Procedures and seven figures and can be found with this article online at https://doi.org/10.1016/j.stemcr.2017.11.005.

AUTHOR CONTRIBUTIONS

J.C.R., A.H.T., L.M.T., A.R.-G., N.R.F., S.M.H., M.S.L., and M.-F.C. designed experiments and analyzed data. J.C.R., A.R.-G., C.C., M.-F.C., M.S.L., and L.M.T. wrote the manuscript. A.H.T., S.Y., A.L., and D.S. performed experiments in R6/2, and J.C.R. performed analyses. S.M.H., C.C., J.A.B., and T.K. performed electrophysiology in R6/2 and analyzed data with guidance from M.S.L. C.M. performed EM with guidance from C.K.M. A.R.-G., N.R.F., and C.Z. performed experiments in Q140, and A.H. analyzed data with guidance from N.R.F. and M.-F.C. J.O. and J.S.S. conducted western blots and analysis. A.K. cultured hNSCs at UCI. B.F., D.C.-B., and G.B. supplied ESI-017 hNSCs and characterizations from the GMP facility at UCD. F.M.L. and M.B.-J. provided advice on experimental design and interpretation of results.

ACKNOWLEDGMENTS

We thank Drs. Laurie Galvan, Ana Maria Estrada-Sánchez, and Elissa J. Donzis for assistance in electrophysiology and Eva Morozko, Phuong Nguyen, Catherine J. Wang, Kenia Portillo-Ortiz, Aaron Samuel Lalehzarian, Arpine Galstyan, Katherine Mowris, Daniel Leventhal, and Pedro Henrique Melo Queiroz for technical assistance. We thank BioTime for ESI-017 cell line. Funding was provided by the California Institute for Regenerative Medicine (CIRM ETAII TR2-01841 and Preclinical grant PC1-08117 to L.M.T., M.L., and M.-F.C.), NIH NS41574 (M.S.L.), NIH NS090390 (L.M.T.), NSF (J.O.), and the Janet Westerfield Foundation (J.O.). Additionally, this work was supported by Merit Review #1BX 001643 to C.K.M. from the United States Department of Veterans Affairs Biomedical Laboratory Research and Development. The contents do not represent the views of the U.S. Department of Veterans Affairs or the United States Government. We also thank UCI Institute for Memory Impairments and Neurological Disorders, Sue and Bill Gross Stem Cell Center, and Optical Biology Shared Resource of the Cancer Center (support grant CA-62203) at the University of California, Irvine for facilities and assistance in carrying out studies.

Received: March 3, 2017
Revised: November 3, 2017
Accepted: November 3, 2017
Published: December 7, 2017

REFERENCES

Ager, R.R., Davis, J.L., Agazaryan, A., Benavente, F., Poon, W.W., LaFerla, F.M., and Blurton-Jones, M. (2015). Human neural stem cells improve cognition and promote synaptic growth in two complementary transgenic models of Alzheimer's disease and neuronal loss. Hippocampus *25*, 813–826.

An, M.C., Zhang, N., Scott, G., Montoro, D., Wittkop, T., Mooney, S., Melov, S., and Ellerby, L.M. (2012). Genetic correction of Huntington's disease phenotypes in induced pluripotent stem cells. Cell Stem Cell *11*, 253–263.

Andre, V.M., Cepeda, C., Fisher, Y.E., Huynh, M., Bardakjian, N., Singh, S., Yang, X.W., and Levine, M.S. (2011). Differential electrophysiological changes in striatal output neurons in Huntington's disease. J. Neurosci. *31*, 1170–1182.

Benraiss, A., Wang, S., Herrlinger, S., Li, X., Chandler-Militello, D., Mauceri, J., Burm, H.B., Toner, M., Osipovitch, M., Jim Xu, Q., et al. (2016). Human glia can both induce and rescue aspects of disease phenotype in Huntington disease. Nat. Commun. *7*, 11758.

Blurton-Jones, M., Kitazawa, M., Martinez-Coria, H., Castello, N.A., Muller, F.J., Loring, J.F., Yamasaki, T.R., Poon, W.W., Green, K.N., and LaFerla, F.M. (2009). Neural stem cells improve cognition via BDNF in a transgenic model of Alzheimer disease. Proc. Natl. Acad. Sci. USA *106*, 13594–13599.

Cepeda, C., Hurst, R.S., Calvert, C.R., Hernandez-Echeagaray, E., Nguyen, O.K., Jocoy, E., Christian, L.J., Ariano, M.A., and Levine, M.S. (2003). Transient and progressive electrophysiological alterations in the corticostriatal pathway in a mouse model of Huntington's disease. J. Neurosci. *23*, 961–969.

Cepeda, C., Wu, N., Andre, V.M., Cummings, D.M., and Levine, M.S. (2007). The corticostriatal pathway in Huntington's disease. Prog. Neurobiol. *81*, 253–271.

Chen, A., Xiong, L.J., Tong, Y., and Mao, M. (2013). Neuroprotective effect of brain-derived neurotrophic factor mediated by autophagy through the PI3K/Akt/mTOR pathway. Mol. Med. Rep. *8*, 1011–1016.

Cicchetti, F., Lacroix, S., Cisbani, G., Vallieres, N., Saint-Pierre, M., St-Amour, I., Tolouei, R., Skepper, J.N., Hauser, R.A., Mantovani, D., et al. (2014). Mutant huntingtin is present in neuronal grafts in Huntington disease patients. Ann. Neurol. *76*, 31–42.

Cummings, D.M., Andre, V.M., Uzgil, B.O., Gee, S.M., Fisher, Y.E., Cepeda, C., and Levine, M.S. (2009). Alterations in cortical excitation and inhibition in genetic mouse models of Huntington's disease. J. Neurosci. *29*, 10371–10386.

Cummings, D.M., Alaghband, Y., Hickey, M.A., Joshi, P.R., Hong, S.C., Zhu, C., Ando, T.K., Andre, V.M., Cepeda, C., Watson, J.B., et al. (2012). A critical window of CAG repeat-length correlates with phenotype severity in the R6/2 mouse model of Huntington's disease. J. Neurophysiol. *107*, 677–691.

Drouin-Ouellet, J. (2014). The potential of alternate sources of cells for neural grafting in Parkinson's and Huntington's disease. Neurodegener. Dis. Manag. *4*, 297–307.

Ebert, A.D., Barber, A.E., Heins, B.M., and Svendsen, C.N. (2010). Ex vivo delivery of GDNF maintains motor function and prevents neuronal loss in a transgenic mouse model of Huntington's disease. Exp. Neurol. *224*, 155–162.

El-Akabawy, G., Rattray, I., Johansson, S.M., Gale, R., Bates, G., and Modo, M. (2012). Implantation of undifferentiated and pre-differentiated human neural stem cells in the R6/2 transgenic mouse model of Huntington's disease. BMC Neurosci. *13*, 97.

Franklin, K., and Paxinos, G. (2007). The Mouse Brain in Stereotaxic Coordinates, Third Edition (Academic Press).

Golas, M.M., and Sander, B. (2016). Use of human stem cells in Huntington disease modeling and translational research. Exp. Neurol. *278*, 76–90.

Goldberg, N.R., Caesar, J., Park, A., Sedgh, S., Finogenov, G., Masliah, E., Davis, J., and Blurton-Jones, M. (2015). Neural stem cells rescue cognitive and motor dysfunction in a transgenic model of dementia with lewy bodies through a BDNF-dependent mechanism. Stem Cell Rep. *5*, 791–804.

Goldberg, N.R., Marsh, S.E., Ochaba, J., Shelley, B.C., Davtyan, H., Thompson, L.M., Steffan, J.S., Svendsen, C.N., and Blurton-Jones, M. (2017). Human neural progenitor transplantation rescues behavior and reduces alpha-synuclein in a transgenic model of dementia with Lewy bodies. Stem Cells Transl. Med. *6*, 1477–1490.

Hickey, M.A., and Chesselet, M.F. (2003). The use of transgenic and knock-in mice to study Huntington's disease. Cytogenet. Genome Res. *100*, 276–286.

Hickey, M.A., Gallant, K., Gross, G.G., Levine, M.S., and Chesselet, M.F. (2005). Early behavioral deficits in R6/2 mice suitable for use in preclinical drug testing. Neurobiol. Dis. *20*, 1–11.

Hickey, M.A., Kosmalska, A., Enayati, J., Cohen, R., Zeitlin, S., Levine, M.S., and Chesselet, M.F. (2008). Extensive early motor and non-motor behavioral deficits are followed by striatal neuronal loss in knock-in Huntington's disease mice. Neuroscience *157*, 280–295.

Hickey, M.A., Zhu, C., Medvedeva, V., Franich, N.R., Levine, M.S., and Chesselet, M.F. (2012a). Evidence for behavioral benefits of early dietary supplementation with CoEnzymeQ10 in a slowly progressing mouse model of Huntington's disease. Mol. Cell Neurosci. *49*, 149–157.

Hickey, M.A., Zhu, C., Medvedeva, V., Lerner, R.P., Patassini, S., Franich, N.R., Maiti, P., Frautschy, S.A., Zeitlin, S., Levine, M.S., et al. (2012b). Improvement of neuropathology and transcriptional deficits in CAG 140 knock-in mice supports a beneficial effect of dietary curcumin in Huntington's disease. Mol. Neurodegener. *7*, 12.

Hockly, E., Woodman, B., Mahal, A., Lewis, C.M., and Bates, G. (2003). Standardization and statistical approaches to therapeutic trials in the R6/2 mouse. Brain Res. Bull. *61*, 469–479.

Kirkeby, A., Parmar, M., and Barker, R.A. (2017). Strategies for bringing stem cell-derived dopamine neurons to the clinic: a European approach (STEM-PD). Prog. Brain Res. *230*, 165–190.

Laforet, G.A., Sapp, E., Chase, K., McIntyre, C., Boyce, F.M., Campbell, M., Cadigan, B.A., Warzecki, L., Tagle, D.A., Reddy, P.H., et al. (2001). Changes in cortical and striatal neurons predict behavioral and electrophysiological abnormalities in a transgenic murine model of Huntington's disease. J. Neurosci. *21*, 9112–9123.

Mangiarini, L., Sathasivam, K., Seller, M., Cozens, B., Harper, A., Hetherington, C., Lawton, M., Trottier, Y., Lehrach, H., Davies, S.W., et al. (1996). Exon 1 of the HD gene with an expanded CAG repeat is sufficient to cause a progressive neurological phenotype in transgenic mice. Cell *87*, 493–506.

Menalled, L.B., Sison, J.D., Dragatsis, I., Zeitlin, S., and Chesselet, M.F. (2003). Time course of early motor and neuropathological anomalies in a knock-in mouse model of Huntington's disease with 140 CAG repeats. J. Comp. Neurol. *465*, 11–26.

Mu, S., Wang, J., Zhou, G., Peng, W., He, Z., Zhao, Z., Mo, C., Qu, J., and Zhang, J. (2014). Transplantation of induced pluripotent stem cells improves functional recovery in Huntington's disease rat model. PLoS One *9*, e101185.

Ochaba, J., Monteys, A.M., O'Rourke, J.G., Reidling, J.C., Steffan, J.S., Davidson, B.L., and Thompson, L.M. (2016). PIAS1 regulates mutant Huntingtin accumulation and Huntington's disease-associated phenotypes in vivo. Neuron *90*, 507–520.

Petit, G.H., Olsson, T.T., and Brundin, P. (2014). The future of cell therapies and brain repair: Parkinson's disease leads the way. Neuropathol. Appl. Neurobiol. *40*, 60–70.

Pollock, K., Dahlenburg, H., Nelson, H., Fink, K.D., Cary, W., Hendrix, K., Annett, G., Torrest, A., Deng, P., Gutierrez, J., et al. (2016). Human mesenchymal stem cells genetically engineered to overexpress brain-derived neurotrophic factor improve outcomes in Huntington's disease mouse models. Mol. Ther. *24*, 965–977.

Richter, F., Gabby, L., McDowell, K.A., Mulligan, C.K., De La Rosa, K., Sioshansi, P.C., Mortazavi, F., Cely, I., Ackerson, L.C., Tsan, L., et al. (2017). Effects of decreased dopamine transporter levels on nigrostriatal neurons and paraquat/maneb toxicity in mice. Neurobiol. Aging *51*, 54–66.

Ross, C.A., and Tabrizi, S.J. (2011). Huntington's disease: from molecular pathogenesis to clinical treatment. Lancet Neurol. *10*, 83–98.

Rosser, A.E., and Bachoud-Levi, A.C. (2012). Clinical trials of neural transplantation in Huntington's disease. Prog. Brain Res. *200*, 345–371.

Rossignol, J., Fink, K.D., Crane, A.T., Davis, K.K., Bombard, M.C., Clerc, S., Bavar, A.M., Lowrance, S.A., Song, C., Witte, S., et al. (2015). Reductions in behavioral deficits and neuropathology in the R6/2 mouse model of Huntington's disease following transplantation of bone-marrow-derived mesenchymal stem cells is dependent on passage number. Stem Cell Res. Ther. *6*, 9.

Simmons, D.A., Rex, C.S., Palmer, L., Pandyarajan, V., Fedulov, V., Gall, C.M., and Lynch, G. (2009). Up-regulating BDNF with an ampakine rescues synaptic plasticity and memory in Huntington's disease knockin mice. Proc. Natl. Acad. Sci. USA *106*, 4906–4911.

Spinelli, K.J., Taylor, J.K., Osterberg, V.R., Churchill, M.J., Pollock, E., Moore, C., Meshul, C.K., and Unni, V.K. (2014). Presynaptic alpha-synuclein aggregation in a mouse model of Parkinson's disease. J. Neurosci. *34*, 2037–2050.

Strand, A.D., Baquet, Z.C., Aragaki, A.K., Holmans, P., Yang, L., Cleren, C., Beal, M.F., Jones, L., Kooperberg, C., Olson, J.M., et al.

(2007). Expression profiling of Huntington's disease models suggests that brain-derived neurotrophic factor depletion plays a major role in striatal degeneration. J. Neurosci. *27*, 11758–11768.

The Huntington's Disease Collaborative Research Group (1993). A novel gene containing a trinucleotide repeat that is expanded and unstable on Huntington's disease chromosomes. Cell *72*, 971–983.

Vashishtha, M., Ng, C.W., Yildirim, F., Gipson, T.A., Kratter, I.H., Bodai, L., Song, W., Lau, A., Labadorf, A., Vogel-Ciernia, A., et al. (2013). Targeting H3K4 trimethylation in Huntington disease. Proc. Natl. Acad. Sci. USA *110*, e3027–e3036.

Vonsattel, J.P., and DiFiglia, M. (1998). Huntington disease. J. Neuropathol. Exp. Neurol. *57*, 369–384.

Walker, R.H., Moore, C., Davies, G., Dirling, L.B., Koch, R.J., and Meshul, C.K. (2012). Effects of subthalamic nucleus lesions and stimulation upon corticostriatal afferents in the 6-hydroxydopamine-lesioned rat. PLoS One *7*, e32919.

Watson, M.B., Richter, F., Lee, S.K., Gabby, L., Wu, J., Masliah, E., Effros, R.B., and Chesselet, M.F. (2012). Regionally-specific microglial activation in young mice over-expressing human wildtype alpha-synuclein. Exp. Neurol. *237*, 318–334.

Zuccato, C., Marullo, M., Vitali, B., Tarditi, A., Mariotti, C., Valenza, M., Lahiri, N., Wild, E.J., Sassone, J., Ciammola, A., et al. (2011). Brain-derived neurotrophic factor in patients with Huntington's disease. PLoS One *6*, e22966.